Network Performance of ROADM Architecture Enabled by Novel Wideband-integrated WSS

Network Performance of ROADM Architecture Enabled by Novel Wideband-integrated WSS

Muhammad Umar Masood
Politecnico di Torino, IT
muhammad.masood@polito.it

Ihtesham Khan
Politecnico di Torino, IT
ihtesham.khan@polito.it

Lorenzo Tunesi
Politecnico di Torino, IT
lorenzo.tunesi@polito.com

Bruno Correia
Politecnico di Torino, IT
bruno.dearaujo@polito.it

Enrico Ghillino
Synopsys, Inc., USA
enrico.ghillino@synopsys.com

Paolo Bardella
Politecnico di Torino, IT
paolo.bardella@polito.it

Andrea Carena
Politecnico di Torino, IT
andrea.carena@polito.it

Vittorio Curri
Politecnico di Torino, IT
curri@polito.it

***Abstract*—Nowadays, optical transport and data center networks utilize wavelength-division multiplexing (WDM) and band division multiplexing (BDM) as possible solutions to increase the capacity to support the ever-increasing traffic demand. It is an alternative solution to simple spatial division multiplexing (SDM) intended to utilize more than one fiber per link. In this perspective, we propose a new modular photonic integrated multi-band wavelength selective switch (WSS) to implement a novel reconfigurable optical add-drop multiplexer (ROADM) architecture. The proposed WSS can operate on a broad spectrum range, covering the three S+C+L bands, and is potentially scalable to large numbers of output fibers and routed channels while maintaining a small footprint. We investigated the network performance assessment of the ROADM architecture based on the proposed multi-band WSS on a German network, and a detailed comparison is given for both SDM and BDM solutions. Results show that the increase in network capacity by exploiting more bands in the cost-efficient BDM scenario is quite close to the SDM scenario using existing infrastructure replicated over multiple fibers.**

***Index Terms*—Wideband, Wavelength Selective Switch, Photonic Integrated Circuit, High-capacity Optical Systems**

I. Introduction

The continuous increase in global Internet traffic and the latest technologies, such as 5G and the Internet of Things (IoT), require larger optical network capacity. Service providers aim to deliver more capacity by implementing cost-effective, scalable, and flexible solutions. Currently, modern optical transport is mainly operated with transparent propagation of WDM comb using coherent optical technologies with dual-polarization over the entire C-band in a spectral window of 4.8 THz, with a maximum transmission capacity of about 38.4 Tbps per fiber [1] when employing PM-16QAM. To further increase network capacity, two leading solutions that can be put into operation are exploiting the residual capacity of already installed fibers or adding new capacity by deploying new fibers. The implementation of the SDM paradigm can be based on legacy technology of multi-fiber (MF) solutions, but in the future, it could also be based on multi-core/mode fiber (MMF/MCF) transmission. Today available SDM solutions rely upon the availability of dark fibers or the installation of new ones. This solution is implemented by replicating the mature technology developed over the year for C-band line systems. The other SDM solutions (e.g., MMF and MCF) have potentially higher capabilities, but they imply a complete replacement of the optical transport infrastructure that requires massive CAPEX efforts.

978-1-6654-3540-6/22

On the other hand, BDM exploits the unused spectral portion of the fiber and aims to enable the transmission of WDM channels over the entire available low-loss spectrum, from the O to the L band (1260-1625 nm): it offers a potentially available frequency bandwidth of over 50 THz [2].

The BDM is a potentially cost-effective solution having the ability to enhance the capacity of the existing network infrastructure. The main issue in the BDM solution is the optical amplification. Several amplifier prototypes are now commercially available to operate in the extended-spectrum region [3]. BDM also requires the availability of filtering and switching modules to enable transparent wavelength routing. The key component of the WDM switching architecture is the WSS, which provides independent control and routing of each input channel to one of the fiber outputs. Traditionally, WSSs are implemented by micro-electro-mechanical mirrors (MEMS) and liquid crystal on silicon (LCoS) technology, resulting in devices that are typically bulky and complex to manufacture and maintain [4].

In contrast, the present work proposes a multi-band WSS implementation using the rapidly emerging photonic integrated circuits (PICs) technology that offers a low-cost solution with a small footprint and massive production capacity. The proposed WSS has a modular architecture that can operate over a wide range of the optical spectrum covering the S+C+L bands. The design of the proposed WSS enables the scalability to accommodate more output fibers and a large number of channels with a smaller footprint than conventional MEMS-based solutions. The present analysis only considers the switching functionality of the ROADM (WSS module) architecture without considering the local add/drop module of ROADM shown in Fig. 1. A detailed network performance assessment of the proposed ROADM architecture based on

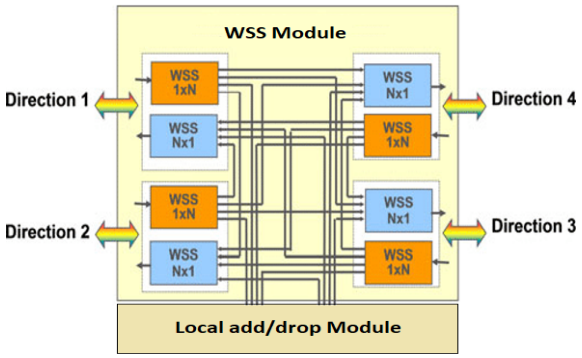

Fig. 1: ROADM architecture enabled by WSSs.

the new multi-band WSS is also demonstrated applying the study to the German network and comparing SDM and BDM solutions. The remainder of this paper is organized as follows. The novel WSS device architecture is described in detail in Section II. Then, the transmission scenario for device analysis is described in Section III. Section IV describes the network scenario and the impact of the proposed WSS solution on network performance. Section V describe the results and Section VI draws some conclusions.

II. Wavelength Selective Switch Architecture

The device under analysis is a photonic integrated circuit (PIC) which enables wavelength-selective switching across a multi-band WDM scenario. The device has been design to target three main band of interest, namely the S+C+L optical communication windows, allowing independent routing of each of the input channel to the required output port. The underlying architecture is modular and scalable, allowing the design for the required number of channels and target output fibers, which can be accomplished without changing the circuit topology. The filtering elements are optimized for the target frequencies in the S+C+L bands, considering a channel separation of 100 GHz. The proposed circuit is shown in Fig. 2, which depicts the overall structure, while highlighting the different operational stages required for the WSS operation. The device achieves the required functionality by dividing the switching and filtering operation into two independent stages: the first section is tasked with the channel separation, extracting each individual channel of the input WDM comb, while the second section is comprised on the parallel switching network and interconnects required to switch the signal to the required output fiber.

The proposed architecture is generalized, as the internal blocks enabling the required switching and filtering operation can be tailored to the desired implementation scenario. The internal components and device technologies proposed in the following sections have been chosen for their design flexibility is the S+C+L bands, although different device solutions could be implemented and tailored for different implementation scenarios.

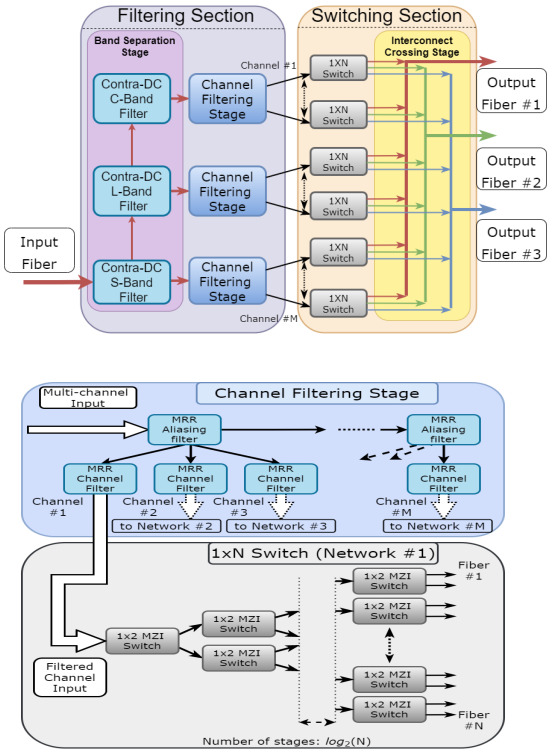

Fig. 2: Circuit model of the proposed WSS structure, highlighting the main operational stages and their block structure.

A. Filtering Section

The first section, as described before, has the goal of separating each channel of the input comb into the various waveguides, while maintaining both losses and cross-talk to a minimum. The proposed integrated solution is based on multiple filtering stages, as to overcome and avoid the main drawback affecting the cross-talk in photonic integrated filters. Due to the periodic nature of the spectral response of such components, the filtering operation must be accomplished in multiple stages, as a simple filter add-drop cascade cannot be suited for a spectrally wide and dense WDM comb.

The first stage of this process consists of separating the S+C+L bands, as to eliminate the inter-band interference, while the second stage selects each individual channel. Two main components have been designed to achieve such results, namely MicroRing Resonator (MRR) filters and Contra-Directional Couplers (CDC). MRRs are one of the standard photonic integrated solutions for implementing add-drop filtering elements, allowing a significant degree of freedom in the design, ranging from simple order blocks to more advanced and efficient higher-order solutions. While the cascade of simpler order filters can improve the spectral properties of the filters, i.e. lower losses and steeper band transitions, the aforementioned period nature of such elements poses a limiting factor when targeting dense WDM scenarios. Simultaneously, MRR solutions are ill-suited for large band-pass applications, such as the band separation required in the proposed structure, due to the physical and technological limitation regarding the

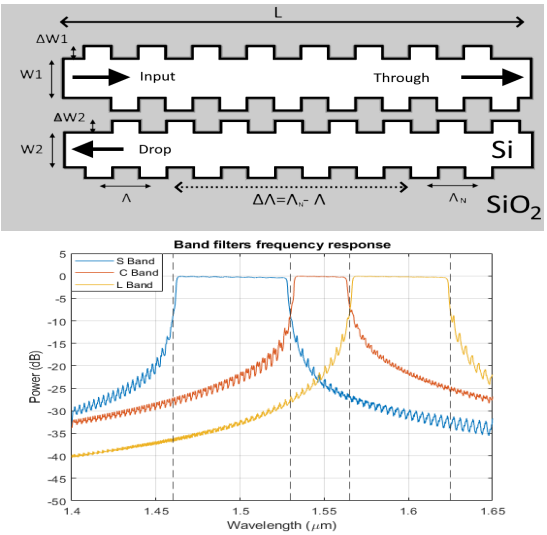

Fig. 3: Contra-Directional Coupler filter: (top) schematic and (bottom) frequency response.

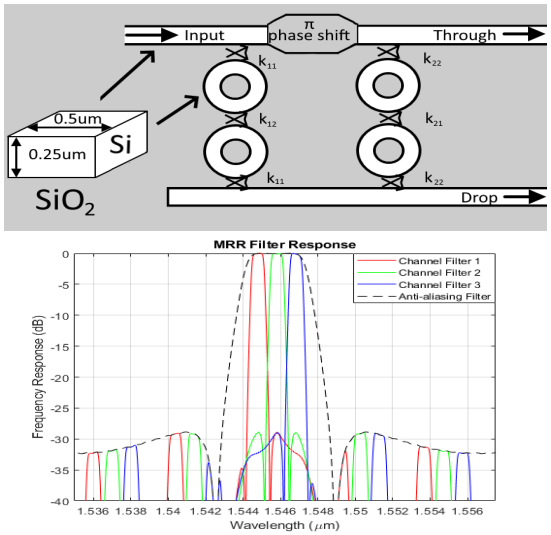

Fig. 4: Device schematic for the two-stage ladder MRR filter. The frequency response is shown for the individual device together with the proposed anti-aliasing solution.

MRR radii. Generally the bandwidth of the filter is inversely proportional to the radius, leading to the described limitation. As such, the first filtering stage is implemented by means of a CDC: while the foot-print of these elements is larger with respect to MRR solutions, wide filtering bandwidth can be easily obtained [5].

The design of the CDC band filters, depicted in Fig. 3, was achieved through coupled-mode theory: by adjusting the grating period, width and chirp, the desired response was obtained in the S+C+L bands, with a flat pass-band profile and a sharp band transition. Solving the band-separation issue, the following filtering stage was implemented through higher order two-stage ladder MRR filters, depicted in Fig. 4. This MRR-based solution is characterized by a flat-top pass-band profile and rapid stop-band transition: the spectral characteristics of the channels make the MRR implementation viable for this second filtering stage, while keeping under control the foot-print of the device. Although the spectral profile of these higher order filters is compatible with the WDM comb, the periodicity must still be taken into account, as to avoid channel interference and aliasing. This can be solved by adding an additional layer, designed with a larger pass-band with respect to the target channel spacing, which acts as an anti-aliasing filter: by combining multiple filters in such a manner, the channel images are filtered out, allowing the extraction of the target channels while minimizing the cross-talk. The depicted frequency response represents a solution for the periodicity issue, although different trade-offs can be made depending on the target implementation, the number of channels, or the footprint constraints. The general principle of operation consists of combining multiple frequency responses as to select only one individual channel between the respective images in the range of interest, which depends on the number of expected channels for the given implementation scenario. In this context the S+C+L band filters allow a reduction of the number of MRR-based elements that would be required to extract an individual channel without experiencing severe aliasing and cross-talk.

B. Switching Section

After the previous filtering stage, each individual channel is routed through an independent switching network, which can propagate it to any of the output fibers. These sub-networks, already depicted in Fig. 2, are implemented as parallel 1×N switches, which can be built by cascading 1×2 Optical Switching Elements (OSE). The elementary 1×2 OSE has been chosen as it represents the standard building block for more complex and higher order photonic switching networks. The switch architecture allows at the same time scalability to any given number of output fiber.

For our analysis this element has been modeled as a Mach-Zehnder Interferometer (MZI) switch. MZI solutions are a standard solution for thermally-controlled switches in photonic integrated solutions, as they allow large flat response, ideal for frequency-independent switching [6]. MZI-based switches can be easily designed to target the operating region of interest, and offer a low-loss solution for such operation, as depicted in Fig. 5 for a C-band centered switch. The switching operation can be achieved through an electrical control signal that heats one of the arms of the MZI, introducing a $\Delta\phi = 90$ shift between the signals in the two waveguides of the device. As shown in Fig. 5 the MZI-based solution can provide the required flat response over a large bandwidth, and can be designed to cover also the S and L bands: the switching sub-networks can be individually tailored to each target channel, allowing a flat response over the whole spectrum [7].

After the switching operation, each channel propagates through the following waveguide crossing layer, which is simply tasked with connecting the output of the switching sub-networks to the respective output port. In this stage each crossing has been considered as a lossy element introduc-

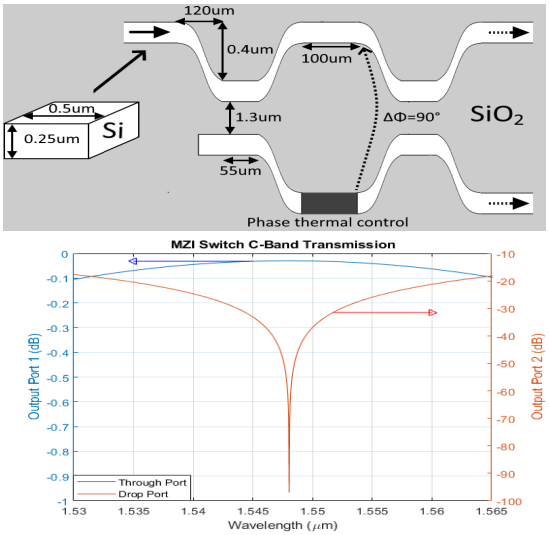

Fig. 5: Schematic and frequency response of the MZI-based switch used in the switching modules.

ing 0.045 dB of insertion loss across the whole considered spectrum. The approximation to a flat value has been chosen as a more detailed characterization would require an in-depth study of the actual circuit footprint and topology for a given implementation, considering the specific waveguide technology and also losses introduced by the bent segment.

III. WDM TRANSPORT LAYER

In order to characterize the penalty of the proposed WSS architecture in a transmission scenario, we developed a simulation model of the device, considering a target implementation with 30 channels distributed in a 100 GHz spaced WDM comb (10 channels in each band), with 3 possible output fibers. The channels are simulated considering dual-polarization 16-QAM modulation format with a symbol rate R_s = 60 GBaud, following the 400ZR standard [8]. The model was built in the Optsim Photonic Circuit Simulation Suite, using simulation results of the internal components to create the circuit blocks required. The transmission and receiver modules were developed and implemented through the DSP library available in the simulation suite. The OSNR penalty was chosen as the Quality-of-Transmission (QoT) metric, evaluated for a reference Bit-Error Rate $\mathrm{BER_{th}} = 10^{-3}$.

The penalty of the proposed architecture is caused by two main contributions: the path-independent filtering and switching and the path-dependent crossing. The filtering and switching component can be considered as the base penalty experienced by each channel independently of the routing state of the WSS, due to the intrinsic loss and cross-talk introduced by the parallel filtering and switching blocks. Meanwhile, the amount of crossing elements encountered by a given channel depends on the routing configuration; as such, a path-dependent loss can be measured and predicted based on the topology of the interconnect stage. Fig. 6 depicts the topology of the proposed case-study, as well as the overall distribution

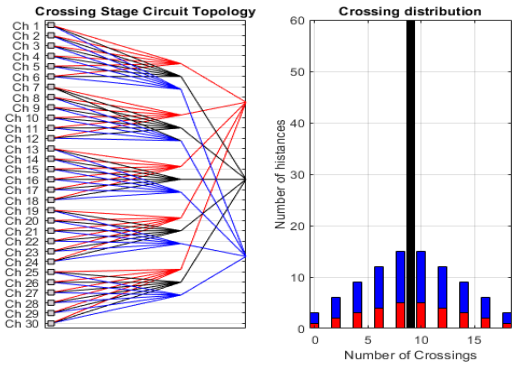

Fig. 6: Interconnect stage topology and distribution of the encountered number of waveguide crossing by each channel.

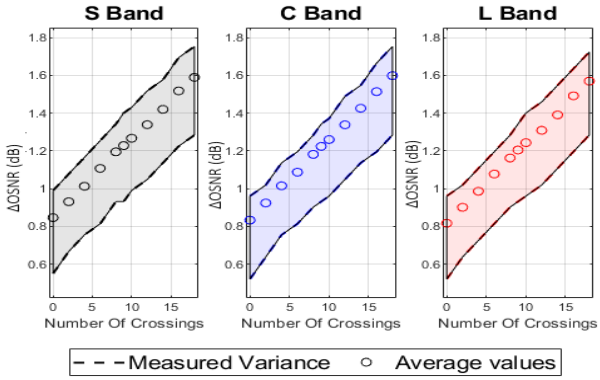

Fig. 7: ΔOSNR penalty distribution for the 10 test channels over the S+C+L bands

of the number of crossing elements, with colors highlighting the different output ports.

By representing penalties as a function of the number of encountered crossings the trend becomes apparent, as depicted in Fig. 7: overall similar penalties are seen in all the three bands, due to the optimization of the designed elements, with a similar variance with respect to the average value.

Based on the obtained simulation results, a general model was built in order to extend the dimension of the device, evaluating the path-dependant penalty based on the circuit topology of the desired implementation. The worst path, corresponding to the higher number of encountered crossings, can be considered as the figure of merit concerning the scalability, depicted in Fig. 8. This value depends on both the number of channels of the input signal, as well as the order of the WSS, or the number of addressable output ports. The expansion of the model through topology-based abstraction represents a good trade-off between penalty estimation and computational time. Fundamentally, the time-domain simulation of the full transceiver considering the DSP for BER extraction in a large scale device is computationally expensive without offering meaningful accuracy improvement. On the other side individual components can be precisely simulated to verify design feasibility and expected performance. At system level, a general penalty-estimation model is necessary, as a rigorous simulation of the losses and penalties would require

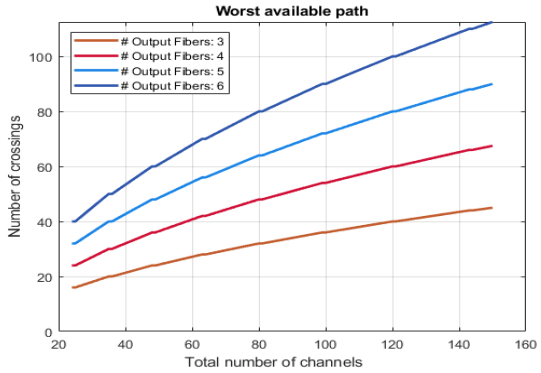

Fig. 8: Number of crossing in the worst path as a function of the number of input channels and number of output fibers (# Output Fibers)

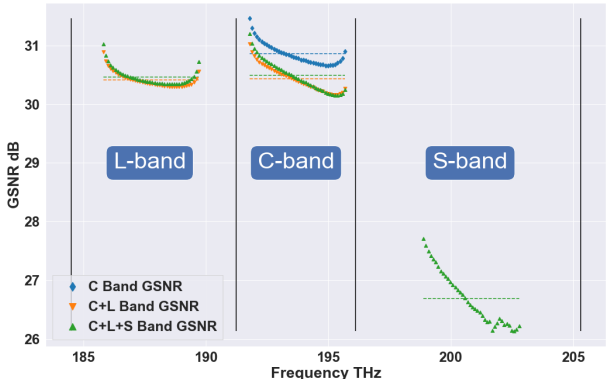

Fig. 9: GSNR vs. frequency for all channels evaluated in each band for all scenarios (C-band only, C+L and C+L+S).

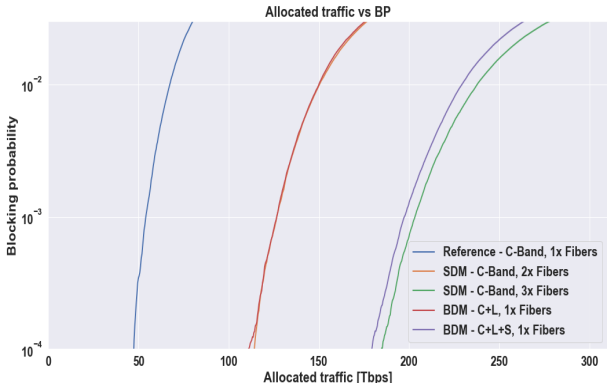

Fig. 10: Blocking probability evaluated over the German network considering ideal transceivers.

a more careful design of actual circuit footprint, considering also manufacturing uncertainty and topology optimization: this analysis, although necessary, is excessively time and resource-intensive at the current level of investigation, as such is not addressed in this study.

IV. Network Performance Assessment

To analyze the impact of the novel WSS architecture on different optical transport solutions, we analyzed the overall network performance. We used the statistic network assessment process (SNAP) [9], which operates at the physical layer of the tested network and is based on the QoT degradation induced by each network element. The QoT metric is in this case the generalized signal-to-noise ratio (GSNR), calculated by taking into account both P_{ASE} and P_{NLI}, using

$$\mathrm{GSNR_i} = \frac{P_{\mathrm{S,i}}}{P_{\mathrm{ASE}(f_i)} + P_{\mathrm{NLI,i}}(f_i)}\,, \tag{1}$$

for the ith channel with central frequency f_i, where $P_{\mathrm{S,i}}$ is the signal launch power, $P_{\mathrm{ASE}(f_i)}$ is the amplified spontaneous emission while $P_{\mathrm{NLI,i}}(f_i)$ is fiber nonlinear interference. We assume that a multi-band optical system is built by a series of bands, with the components, particularly the optical amplifiers, optimized per band [2]. Then we consider that each fiber in the amplified lines has identical lengths of 75 km and fiber type (ITU-T G.652D standard single-mode fiber). For the C- and L-band channels, we use commercial erbium-doped fiber amplifiers (EDFAs), and for the S-band we consider channels amplified with a thulium-doped fiber amplifier (TDFA) [10]. Each band operates on the ITU-T 100 GHz WDM grid with transceivers setting a symbol rate of 60 GBaud.

For the C, L and S bands, with 40 channels in each, an input power optimization has been performed according to a span-by-span strategy, using the local optimization global optimization algorithm (LOGO) based on QoT maximization [11]. The GSNR profile vs. frequency of a fully loaded single span of 75 km for C, C+L and C+L+S bands is shown in Fig. 9. The acquired average GSNR is shown using dotted lines in Fig. 9. The average GSNR of 30.85 dB is obtained when only C-band is used for transmission. When L-band is also put into operation (C+L), the GSNR of the average C-band GSNR is 30.43 dB, and the L-band average GSNR is 30.41 dB, respectively. Now, let's turn the S-band into transmission (C+L+S); in this case, the average GSNR of C-band is 30.48 dB, L-band is 30.46 dB, and for S-band, it is 26.69 dB. Compared with the reference C-band transmission case, the average GSNR of the C-band is reduced in C+L and C+L+S band scenarios due to the NLI and its iteration with the stimulated raman scattering (SRS) effect. Lightpaths are assigned according to the defined routing and wavelength assignment (RWA) algorithm (k-shortest paths with $k = 5$ for routing and first-fit for spectrum allocation) and ZR+ transceiver characteristics [12]. Moreover, the network assessment is done using a uniform traffic distribution among the network nodes. In this work, we have considered the German topology, which consists of 17 optical nodes and 26 edges with an average node degree of 3.1, an average distance between nodes of 207 km, and a maximum link length of 300 km [10]. Network metrics are statistically determined by Monte Carlo analysis.

V. Results and Discussion

To ensure a fair comparison of multi-band results while deploying the ROADM architecture using the proposed WSS structure, we compare BDM to SDM network performance using SNAP, assuming that SDM uses multiple fibers within

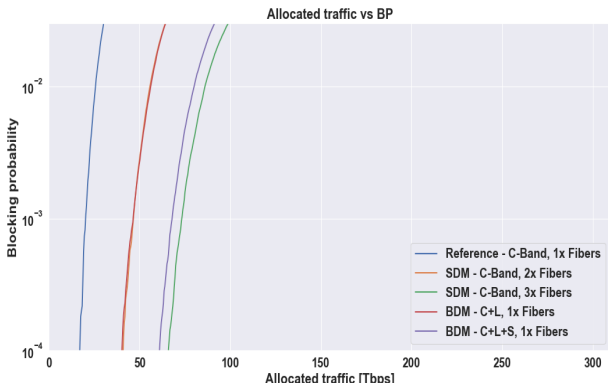

Fig. 11: Blocking probability evaluated over the German network considering realistic ZR+ transceivers.

the C-band on the same total available spectrum. For SDM, we assume a core continuity constraint (CCC) where each LP must be allocated in the same fiber from the source to the destination node, corresponding to the switching technique [13]. This option is preferred since the number of fiber pairs is increased by two and three times compared to the BDM approach with S+C+L.

Optimized transmission results are used to perform network-level analysis, using the GSNR values for each WDM channel to create the topological graph, which is weighted by GSNR degradation to implement SNAP. For each case, SNAP is applied on both ideal (zero-penalty) (Fig. 10) and realistic ZR+ transceivers (Fig. 11). We consider as a reference the C-band 1x fiber and we compare (i) the C-band SDM 2x fibers with the C+L BDM, (ii) the C-band SDM 3x fibers with the C+L+S BDM. Results are shown as a statistical average over the Monte Carlo runs of the blocking probability (BP) versus the total progressively assigned traffic for each BDM and equivalent SDM scenario and for the ideal versus the realistic ZR+ transceiver. Using BP = 10^{-2} as a reference we determine the amount of traffic that can be allocated for each case: this is the comparison metric for the different transmission solutions. In Fig. 10, allocated traffic vs. blocking probability is plotted for ideal transceivers. The C-band 1x fiber deliver ∼65 Tbps. Considering SDM C-band 2x fibers and BDM C+L 1x fiber, they almost perform equally reaching an allocated traffic of ∼150 Tbps. For SDM C-band 3x fiber, we get ∼238 Tbps while for for BDM C+L+S 1x fiber, we get ∼228 Tbps. Fig. 11 shows allocated traffic vs. blocking probability for realistic ZR+ transceivers. The C-band 1x fiber considered as a reference delivers ∼25 Tbps. SDM C-band 2x fibers and BDM C+L 1x fiber again almost perform equally with an allocated traffic of ∼56 Tbps. For SDM C-band 3x fiber, we get ∼87 Tbps while for BDM C+L+S 1x fiber we get ∼80 Tbps. Comparing BDM and SDM solutions, both for ideal and realistic ZR+ transceivers, we found that all BDM solutions performs very close to their respective SDM reference solution. This confirms that multiband transmission is a promising and viable solution to expand network traffic capacity without deploying new fiber infrastructures.

VI. Conclusion

In this work, we proposed a novel modular photonic integrated wideband WSS capable of supporting multi-band operation across different spectral regions, including the S+C+L bands. The proposed multi-band WSS is utilized as a switching section of a ROADM architecture. The presented ROADM architecture performance is assessed in terms of deployed traffic for BDM scenarios: we compared results with equivalent SDM cases. The BDM C+L scenario approximately doubles the capacity of the German network for a target BP of 10^{-2} and it shows same performance level as the SDM approach based on two fibers. In contrast, in the S+C+L scenario, the capacity nearly tripled that of the reference C band case. In this case the SDM solution provides more traffic than BDM. BDM suffers of an increased impact due to non-linear propagation: all channels are in the same fiber. It is still possible to improve BDM, minimizing this difference, with a proper adjustment of launch power for each band, an approach that we did not consider in this paper. In any case the capacity reduction observer in the BDM case is not substantial and it shows that BDM solutions are a potential cost-effective technology for upgrading network capacity without installing new fibers.

References

[1] K. Kim, K.-H. Doo, H. H. Lee, S. Kim, H. Park, J.-Y. Oh, and H. S. Chung, "High speed and low latency passive optical network for 5G wireless systems," JLT **37**, 2873–2882 (2018).

[2] A. Ferrari, A. Napoli, J. K. Fischer, N. Costa, A. D'Amico, J. Pedro, W. Forysiak, E. Pincemin, A. Lord, A. Stavdas *et al.*, "Assessment on the achievable throughput of multi-band ITU-T G. 652. D fiber transmission systems," J. Light. Technol. **38**, 4279–4291 (2020).

[3] V. Curri, "Multiband optical transport: a cost-effective and seamless increase of network capacity," in *PND,* (OSA, 2021), pp. NeTu2C–3.

[4] T. A. Strasser and J. L. Wagener, "Wavelength-selective switches for roadm applications," IEEE JSTQE **16**, 1150–1157 (2010).

[5] M. Hammood, A. Mistry, H. Yun, M. Ma, S. Lin, L. Chrostowski, and N. A. F. Jaeger, "Broadband, silicon photonic, optical add–drop filters with 3 dB bandwidths up to 11 THz," OL **46**, 2738–2741 (2021).

[6] X. Tu, C. Song, T. Huang, Z. Chen, and H. Fu, "State of the art and perspectives on silicon photonic switches," Micromachines **10** (2019).

[7] I. Khan, L. Tunesi, M. U. Masood, E. Ghillino, P. Bardella, A. Carena, and V. Curri, "Optimized management of ultra-wideband photonics switching systems assisted by machine learning," OE **30**, 3989–4004 (2022).

[8] I. Khan, L. Tunesi, M. U. Masood, E. Ghillino, P. Bardella, A. Carena, and V. Curri, "Machine learning assisted accurate estimation of qot impairments of photonics switching system on 400zr," in *ACP 2021,* (Optica Publishing Group, 2021), p. T2B.2.

[9] V. Curri, M. Cantono, and R. Gaudino, "Elastic all-optical networks: A new paradigm enabled by the physical layer. How to optimize network performances?" JLT **35**, 1211–1221 (2017).

[10] B. Correia, R. Sadeghi, E. Virgillito, A. Napoli, N. Costa, J. Pedro, and V. Curri, "Power control strategies and network performance assessment for C+L+S multiband optical transport," JOCN **13**, 147–157 (2021).

[11] V. Curri, A. Carena, A. Arduino, G. Bosco, P. Poggiolini, A. Nespola, and F. Forghieri, "Design strategies and merit of system parameters for uniform uncompensated links supporting Nyquist-WDM transmission," JLT **33**, 3921–3932 (2015).

[12] Implementation agreement for a 400ZR coherent optical interface, https://www.oiforum.com/technical-work/hot-topics/400zr-2/.

[13] P. S. Khodashenas, J. M. Rivas-Moscoso, D. Siracusa, F. Pederzolli, B. Shariati, D. Klonidis, E. Salvadori, and I. Tomkos, "Comparison of spectral and spatial super-channel allocation schemes for sdm networks," JLT **34**, 2710–2716 (2016).